Available online at www.sciencedirect.com
ScienceDirect
International Journal of Mass Spectrometry 258 (2006) 50–57
International Journal of Mass Spectrometry
www.elsevier.com/locate/ijms

Airborne nanoparticle characterization with a digital ion trap–reflectron time of flight mass spectrometer

Shenyi Wang, Murray V. Johnston *

Department of Chemistry and Biochemistry, University of Delaware, Newark, DE 19716, USA

Received 5 April 2006; received in revised form 29 June 2006; accepted 3 July 2006
Available online 4 August 2006

Abstract

A digital ion trap–reflectron time of flight mass spectrometer is described for airborne nanoparticle characterization. Charged particles sampled into this nanoaerosol mass spectrometer (NAMS) are captured in the ion trap and ablated with a high fluence laser pulse to reach the "complete ionization limit". Atomic ions produced from the trapped particle(s) are mass analyzed by time of flight, and the elemental composition is determined from the relative signal intensities in the mass spectrum. The particle size range captured in the ion trap is selected by the frequency applied to the ring electrode. Size selection is based on the mass normalized particle diameter, defined as the diameter of a spherical particle with unit density that has the same mass as the particle being analyzed. For the current instrument configuration, ring electrode frequencies between 5 and 140 kHz allow selective trapping of particles with a mass normalized diameter between 7 and 25 nm with a geometric standard deviation of about 1.1. The particle detection efficiency, defined as the fraction of charged particles entering the mass spectrometer that are subsequently captured and analyzed, is between 1×10^{-4} and 3×10^{-4} over this size range. The effective particle density can be determined from simultaneous measurement of the mobility and mass normalized diameters. Test nanoparticles composed of sucrose, polyethylene glycol, polypropylene glycol, sodium chloride, ammonium sulfate and copper(II) chloride are investigated. In most cases, the measured elemental compositions match the expected elemental compositions within ±5% or less and the measured compositions do not change with particle size. The one exception is copper chloride, which does not yield a well-developed plasma when it is irradiated by the laser pulse.

Keywords: Nanoparticle; Digital ion trap; Single particle laser ablation; Aerosols

1. Introduction

Airborne particles in the 1–100 nm diameter range have been referred to as "ultrafine" particles if they are a side product of natural or anthropogenic activities, or "nanoparticles" if they are synthesized for nanotechnological applications. Increasingly, the term "nanoparticle" is used for both types of particles. Particles at the low end of the size range have a similar dimension to individual macromolecules, while particles at the high end of the size range may be individual particles that have grown in size by condensation of nonvolatile material or aggregation of smaller particles. Chemical characterization of airborne nanoparticles is important as they may have significant impacts on human health and global climate [1–3], but it is also difficult because of the small mass involved. For example, a single 10 nm diameter particle contains on the order of 10^{-18} g and the number concentration in ambient air ranges from 10^2 to 10^5 particles/cm^3.

On-line, real-time characterization of the size and composition of airborne nanoparticles presents two significant analytical challenges: (1) efficient sampling of particles in a size-selective manner and (2) sensitive detection and analysis of the small mass involved. Recently, we described a nanoaerosol mass spectrometer (NAMS) capable of meeting these challenges [4]. Charged particles enter the mass spectrometer through an aerodynamic inlet and are transmitted through an ion guide with the aid of static and dynamic electric fields. The particles subsequently enter a quadrupole ion trap where they are captured and focused to the center of the trap. A high energy pulsed laser beam is also focused to the center of the trap to disintegrate the captured particle(s) into multiply charged atomic ions. The ions are mass analyzed by time of flight. The method was demonstrated with particles and macromolecules in a specific sub-10-nm size range.

* Corresponding author. Tel.: +1 302 831 8014; fax: +1 302 831 6335.
E-mail address: mvj@udel.edu (M.V. Johnston).

1387-3806/$ – see front matter © 2006 Elsevier B.V. All rights reserved.
doi:10.1016/j.ijms.2006.07.001

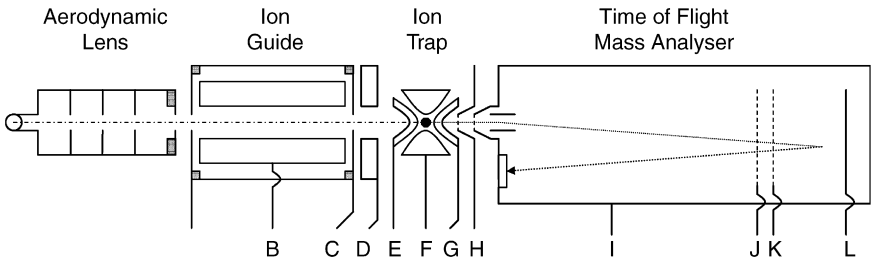

Fig. 1. Schematic of the nanoaerosol mass spectrometer. Components A–L are identified in the text. Trapped particles are irradiated in the center of the ion trap, denoted by a black dot.

We report here continued development of the NAMS for nanoparticle analysis. In particular, the sinusoidal potential applied to the ring electrode of the ion trap is replaced by a rectangular (square wave) potential. This so-called "digital ion trap" (DIT) has advantages of simplicity and versatility relative to a conventional sinusoidal quadrupole ion trap (QIT). Time varying potentials are generated with off-the-shelf components without the need to design a custom sinusoidal power supply. Adjusting the amplitude, frequency and constant potential offset are straightforward, making it easy to manipulate the size range of particles that are captured.

The stability criteria for ion motion in a periodic rectangular potential was investigated in the early 1970s by Richards et al. [5]. More recently, Ding et al. [6–8] have extended this work to the development of a DIT in which externally generated ions from an atmospheric pressure source are injected into the trap and mass analyzed. Operating parameters for the DIT were studied with respect to both the efficiency of external ion trapping and the attainment of high resolving power during a mass scan. In the NAMS instrument described here, the DIT serves only one function—to trap charged particles that can be thought of as very high m/z (megadalton) ions. Mass analysis is performed separately by ejecting (low m/z) atomic/molecular ions from the trap into a time of flight (TOF) mass analyzer. As will be shown, in addition to simplicity of operation, the DIT–TOF combination provides a relatively wide particle size range for size-selective trapping and analysis.

2. Experimental methods

The general design of the instrument is similar to our previous work [4] although several modifications have been made. Fig. 1 shows the configuration used in this work. Table 1 summarizes the operating conditions for the components identified in Fig. 1. Prior to entering the mass spectrometer, the aerosol is brought to an equilibrium charge distribution with a radioactive neutralizer (NRD LLC, Grand Island, NY). About 5% of the particles receive a single charge of the desired polarity (positive). Most of the remaining particles are uncharged; no multiply charged particles are generated in the size range studied here. The aerosol enters the mass spectrometer through a flow limiting orifice at 82 cm^3/min and is focused through an aerodynamic lens/nozzle assembly designed for transmitting particles under 30 nm in diameter ("nanoparticle lens A" in ref. [9]). The pressure inside the aerodynamic lens assembly is 3 Torr. After exiting the nozzle, the particle beam traverses a 6 mm long differentially pumped region held at $\sim 7 \times 10^{-3}$ mbar by a turbomolecular pump. At the end of this region is a quadrupole ion guide (B) consisting of four cylindrical rods (10 mm diameter, 12 cm length, $r_o = 4$ mm) bounded by two 1 mm diameter apertures. An argon gas leak into the ion guide maintains a pressure of $\sim 2.5 \times 10^{-2}$ mbar. The entrance aperture (A) is held at ground and the exit aperture at −2 V (C). The sinusoidal potential applied to the rods (140 kHz; 800 $V_{p\text{-}p}$) is provided by a custom-built power supply (Pacific Northwest National Laboratory, Richland, WA). Focusing lens D (4 mm diameter, 5 mm wide) is positioned 1.25 mm after the exit aperture of the ion guide and 12 mm before the entrance aperture to the quadrupole ion guide. The optimum voltage applied to this lens changes with particle size, from about −40 V in the 10 nm region to −200 V in the 20 nm region.

The quadrupole ion trap–reflectron time of flight mass analyzer is similar to the standard design provided by R.M. Jordan Co. (Grass Valley, CA). The particle beam enters through one end cap (E) and ions produced by laser irradiation are accel-

Table 1
Typical operating conditions for NAMS

Component[a]	Operating condition	Component[a]	Operating condition
A	0 V	G	−2 V accumulation; −500 V pulse extraction
B	140 kHz, 800 $V_{p\text{-}p}$ sinusoidal	H	−1160 V
C	−2 V	I	−1200 V
D	0 to −200 V	J	−1200 V
E	−2 V accumulation; +1300 V pulse extraction	K	−175 V
F	4–150 kHz; −508/+504 V square wave	L	+510 V

[a] Components are identified in Fig. 1.

erated into the reflectron time of flight mass analyzer through the opposite end cap (G). The laser beam enters and exits through openings drilled in the ring electrode (F). The ion trap ($r_o = 10$ mm; $z_o = 7.1$ mm) is maintained at as high a pressure as possible ($\sim 10^{-4}$ mbar measured at the gauge; pressure in the trap is expected to be at least an order of magnitude higher) with an argon gas leak through a pulsed valve with a response time of 2 ms (Series 9, Parker Hannifin Corporation, Fairfield, NJ). The valve remains open during the particle accumulation time period and closes 30 ms before the laser fires. This sequence maximizes the pressure during particle accumulation and provides a significantly lower pressure during ion extraction.

The potential applied to the ring electrode is provided by a high speed, high voltage pulser (Model PVX-4150, Directed Energy, Inc., Ft. Collins, CO) driven by a square wave generator (Model DS345, Stanford Research Systems, Sunnyvale, CA) and two high voltage power supplies (Model SL300, Spellman, Hauppauge, NY). Normally, amplitudes of +504 and −508 V are used, giving a "float" potential of −2 V. The maximum voltage that can be applied to the electrode without breakdown is 750 V. The frequency is varied from about 4 to 150 kHz. Higher frequencies are difficult to generate with large amplitudes owing to the capacitance of the ion trap and connecting cable (80 pF total). During particle accumulation, both end caps are kept at −2 V. Just before the laser fires, end cap E is pulsed to +1300 V and end cap G to −500 V, each with a duration of 20 μs. The laser pulse coincides with the positive voltage of the square wave applied to the ring electrode (i.e., +504 V).

Ions produced by the laser pulse exit the end cap, pass through focusing lens H (−1160 V) and into the flight tube I (1 m length, floated at −1200 V). The potentials applied to the reflectron at the rear end of the flight tube are typically −1200 V (J), −175 V (K) and +510 V (L), although proportionally lower voltages for K and L are sometimes used. The effect of reflectron voltage on the mass spectrum is discussed below. The flight tube is differentially pumped to achieve a base pressure of 10^{-6} mbar.

Trapped particles are ablated with a Nd:YAG laser at 532 nm (Model CFR 400, Big Sky Lasers, Bozeman, MT). The laser radiation is focused with a 75 mm f.l. lens to an approximate diameter of 0.5 mm and the pulse energy inside the ion trap is 160 mJ. The laser is triggered by the square wave that generates the ring electrode potential. The laser is normally pulsed around 3 Hz. For example, if the ring electrode frequency is 40 kHz, the laser is fired once every 13,333 cycles. If a constant laser repetition rate is desired, then the division rate must change with the ring electrode frequency. A particle is considered "hit" and the mass spectrum saved when the ion signal in the *m/z* range of interest increases above a threshold level. Fig. 2 shows a timing diagram for the laser pulse and potentials E, F and G.

Particles are produced from aqueous solutions of analyte using an electrospray aerosol generator (Model 3480, TSI, Inc., Shoreview, MN). If the solute is nonconducting, then ammonium acetate is added to achieve an adequate conductivity. Particle size distributions and number concentrations are measured with a scanning mobility particle sizer (nanoSMPS–TSI, Inc., Shoreview, MN).

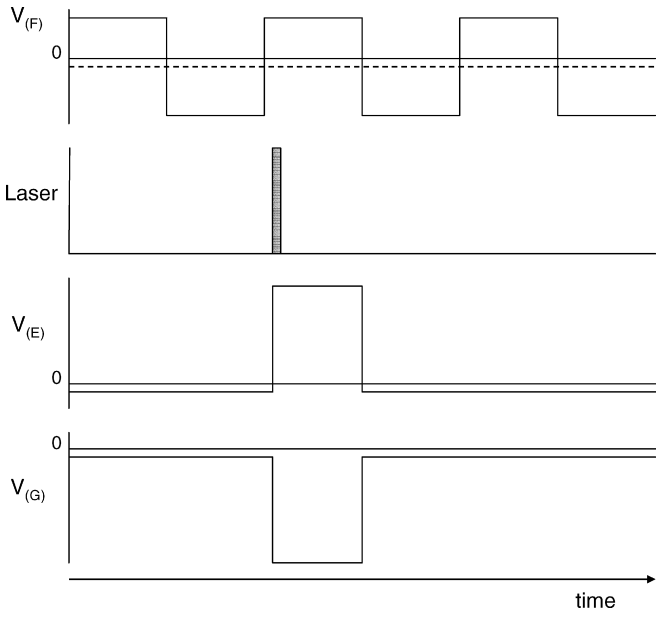

Fig. 2. Timing diagram for the laser pulse and voltages E–G. The float potential for voltages E–G is −2 V.

3. Results and discussion

3.1. Particle trapping

In our previous work [4], we showed that particles could be size selectively captured in the ion trap. In that work, changing the particle size was difficult owing to the electronics used to generate the sinusoidal potential for the ring electrode. As will be shown below, changing the frequency and/or amplitude of the ring electrode potential is straightforward with the digital ion trap. Investigating the size selectivity of particle trapping requires the use of a scanning mobility particle sizer (SMPS) to measure and/or select the particle size produced from the electrospray particle generator. The SMPS selects particles on the basis of mobility diameter, d_m. In contrast, the ion trap selects particles on the basis of *m/z* where $z = 1$ for the size range of interest. To relate the two, we define the mass normalized diameter, d_{mn}, which is the diameter of a spherical particle with unit density (1 g/cm^3) that contains the same mass as the particle being selected by the SMPS:

$$d_{mn} = \rho_p^{1/3} d_m \quad (1)$$

where ρ_p is the effective density of the particle being analyzed. If there are no internal voids in the particle, the particle is spherical and the nanoparticle structure is the same as the structure of a bulk sample, then ρ_p is given by the bulk density. If the particle is nonspherical, then ρ_p in Eq. (1) will be smaller than the bulk density. In the work described below, sucrose test particles are characterized. The shape is assumed to be spherical [10] and the density equal to the bulk value (1.58 g/cm^3). Particles with d_m between 8.5 and 21.5 nm are analyzed, which corresponds to d_{mn} between 9.9 and 25.0 nm. In addition, a mixture of bovine serum albumin monomers and dimers is characterized. These particles have an average d_m of 7.1 nm, and based on the effective

densities reported by Kaufman et al. [11], d_{mn} is about the same as d_m.

The stability criteria for ion motion in a DIT are similar though not identical to those for a conventional QIT [6,7]. Under conditions where $a_z = 0$, q_z must be less than 0.712 for stable motion in the DIT:

$$q_z = \frac{4eV}{mr_o^2(2\pi f)^2} = \frac{(6 \times 10^{-3})eV}{\pi^3 d_{mn}^3 r_o^2 f^2} \leq 0.712 \quad (2)$$

where r_o is the trap radius, V and f are the amplitude and frequency of the ring electrode potential, the particle is assumed to have a single positive charge, and MKS units are used throughout. Eq. (2) suggests for a given amplitude and frequency, all particle diameters will be trapped above the minimum diameter for which $q_z = 0.712$. However, one also has to consider the pseudopotential well depth in the trap that is established by the ring electrode potential. For $q_z < 0.3$, the pseudopotential well depth of a digital ion trap (D_z) is given by:

$$D_z \approx 0.206(q_z V) \quad (3)$$

where V is the ring electrode amplitude [7]. For given values of r_o, V and f, Eqs. (2) and (3) show that as the particle diameter increases and q_z decreases, the well depth decreases. Eventually, the well becomes so shallow that particles can no longer be confined to the center of the trap for laser irradiation and analysis. Therefore, there is a finite size range over which particles are trapped. For given values of q_z and V, D_z for the DIT is greater than that for the QIT, which suggests that the DIT will be more effective in trapping large (high m/z) particles.

In the present work, particle trapping is indirectly studied by measurement of the particle detection efficiency (DE), defined as the fraction of charged particles entering the mass spectrometer that are detected and analyzed:

$$DE = \frac{HR}{VN} \quad (4)$$

where HR is the observed hit rate (particles detected and analyzed per minute), V the flow rate of aerosol into the mass spectrometer (cm^3/min) and N is the number concentration (particles/cm^3) measured with the SMPS. DE is a combination of several factors including the transmission efficiency of particles from atmospheric pressure to the DIT, the trapping efficiency of particles in the DIT and the probability that when a particle is irradiated by the pulse laser a measurable ion signal is produced.

The role that the quadrupole ion guide plays in efficiently transmitting particles to the DIT was investigated by comparing the DE obtained under various operating conditions. The gas pressure in the ion guide plays an important role as the DE generally increases with increasing gas pressure, and the effect is more pronounced for large particles. If the electric field is turned off, i.e., the rods B in Fig. 1 are grounded, then the DE is much lower and the magnitude depends on particle size. For 12 nm (d_{mn}) particles, removing the sinusoidal potential from the rods decreases DE by a factor of 100; for 18 nm particles, the decrease is a factor of 35; for 22 nm particles, the decrease is a factor of 6; and for 28–32 nm particles, the decrease is a factor of 4.

We rationalize these observations in the following way. The ion guide is designed to thermalize and electrodynamically focus ca. 10 nm particles [4]. These particles require the greatest amount of focusing because they are light and tend to follow the gas streamlines. The quadrupole ion guide keeps them online so that they are efficiently transmitted to the ion trap. As the particle size (and mass) increases, the particles are more likely to remain online in a collimated beam owing to an increasing aerodynamic focusing effect (and less Brownian motion) in the aerodynamic lens system. At the same time, the electrodynamic focusing in the quadrupole ion guide becomes less effective because the pseudopotential well becomes very shallow. The net effect for large particles is only a slight enhancement of the DE when the sinusoidal potential is applied, but the overall DE remains high (see below) because of improved aerodynamic focusing. The need for a buffer gas in the ion guide for all particle sizes indicates that ion trapping is facilitated by a reduction of the particle velocity, although complete thermalization is not necessary.

Simulations of ion trapping in a QIT by Quarmby and Yost [12] show that the probability of trapping externally generated ions is strongly dependent on the radio frequency phase at the time of ion injection. Furthermore, the optimum value of q_z appears to decrease with increasing m/z, approximately 0.2 for 100 m/z and 0.07 for 1500 m/z. Similar effects are observed in a DIT. Simulations by Ding et al. [6] show that when an ion enters the trap at a proper time point (phase) in the square wave cycle, the secular motion of the ion with respect to changes in the ring potential keeps it confined in the trap. Ion motion in the trap is not stable in that the ion could exit the trap through the entrance aperture. However, if the ion has a sufficient radial velocity, it takes many cycles of motion before the ion "finds" the entrance aperture. During this time, collisional cooling brings the kinetic energy below D_z so that stable motion is achieved and the ion is focused to the center of the trap. Because the potential remains high for a longer portion of a square wave cycle than a sinusoidal cycle and D_z for a given q_z and V is larger for a DIT than a QIT, the probability that an ion can be confined in DIT is apparently greater than that in a QIT. Based on their simulations, Ding et al. conclude that "the DIT with a trapping voltage of only 1 kV has, in many respects, equivalent analytical performance to an r.f. trap with a trapping voltage of 16 kV" [7]. We hypothesize that the ability of large particles to be trapped in the NAMS is a reflection of these unique characteristics of the DIT.

The above explanation for efficient trapping of large particles is consistent with the particle size dependence of lens D in Fig. 1. Ding et al. [6,7] find that the insertion of a field adjusting (FA) electrode just upstream of the DIT greatly increases the efficiency of ion trapping. Optimum trapping occurs when the square wave potential is in the positive half of the cycle and a negative potential is applied to the FA electrode. The net effect of the two opposite polarity potentials is a relatively flat potential gradient in the vicinity of the entrance aperture to the DIT. This allows ions with a kinetic energy below the square wave potential to enter the trap and then be reflected by back toward the entrance by the square wave potential. If the ion has a sufficient radial velocity, it does not reflect straight back to the entrance aperture and becomes confined in the trap. We

suggest that a similar phenomenon occurs for particle trapping in NAMS, where lens D serves the role of the FA electrode. Efficient trapping is observed only when a negative potential is applied to lens D and the magnitude of the optimum potential increases with increasing particle size. While ion confinement and subsequent collisional cooling provides a reasonable explanation for the ability of NAMS to trap relatively large particles, confirmation will require detailed modeling studies. It should be noted that alternative trapping mechanisms, for example inelastic particle bounce off a wall inside the trap, cannot be ruled out at this stage.

Fig. 3a shows a plot of ring electrode frequency versus d_{mn} for the test particles. The square wave amplitude is held constant (+504 and −508 V) and the frequency is varied until the maximum DE is found. The optimum frequency (f_{opt}) is then plotted versus d_{mn}. Fig. 3b shows the q_z values for optimum particle trapping determined from the experimentally measured optimum frequencies. The optimum q_z tends to increase with increasing particle size. This result is not unexpected as a larger value of q_z will give a deeper pseudopotential well depth (Eq. (3)). The well depths corresponding to these values of q_z vary from ∼2 V for the lower sizes to ∼9 V for the larger sizes.

Fig. 3c shows a plot of the optimized DE (determined at f_{opt}) versus d_{mn}. DE appears to increase slightly with increasing particle size. However, it should be noted that DE is a difficult parameter to quantify because it is strongly dependent on several phenomena: (1) the threshold signal level chosen to determine when a particle is "hit" while eliminating "background" triggers; (2) the pulse to pulse stability of the laser, since the absolute signal intensity can vary an order of magnitude with small variations in the laser energy; (3) fluctuations in the buffer gas flow to the ion guide and trap; (4) fluctuations in the particle number concentration and/or size distribution from the electrospray generator (a major factor in this work); and (5) particle counting statistics, which can be unfavorable if the number concentration at the desired particle size is low. In unfavorable situations, repeat measurements of DE can vary by 50% or more. Therefore, it is not surprising that significant scatter is observed in the plots of Fig. 3.

Fig. 4 shows plots of DE versus particle size for three different frequencies. The geometric standard deviations for the three plots are close to 1.1 with perhaps a slight increase with increasing particle size.

3.2. Particle analysis

The laser fluence that irradiates trapped particles is high enough to reach the so-called "complete ionization limit" [13–16]. In this limit, a laser induced plasma is formed and the particle is thought to be completely disintegrated into positively charged atomic ions and electrons. However, when the particle size is small and the ion current from the disintegrated particle is low, "background" signal from processes such as ionization of background gas with electrons from the plasma and/or residual laser radiation striking a metal surface becomes a significant portion of the total ion current [4]. Note that electrons move away from the disintegrated particle much faster than atomic

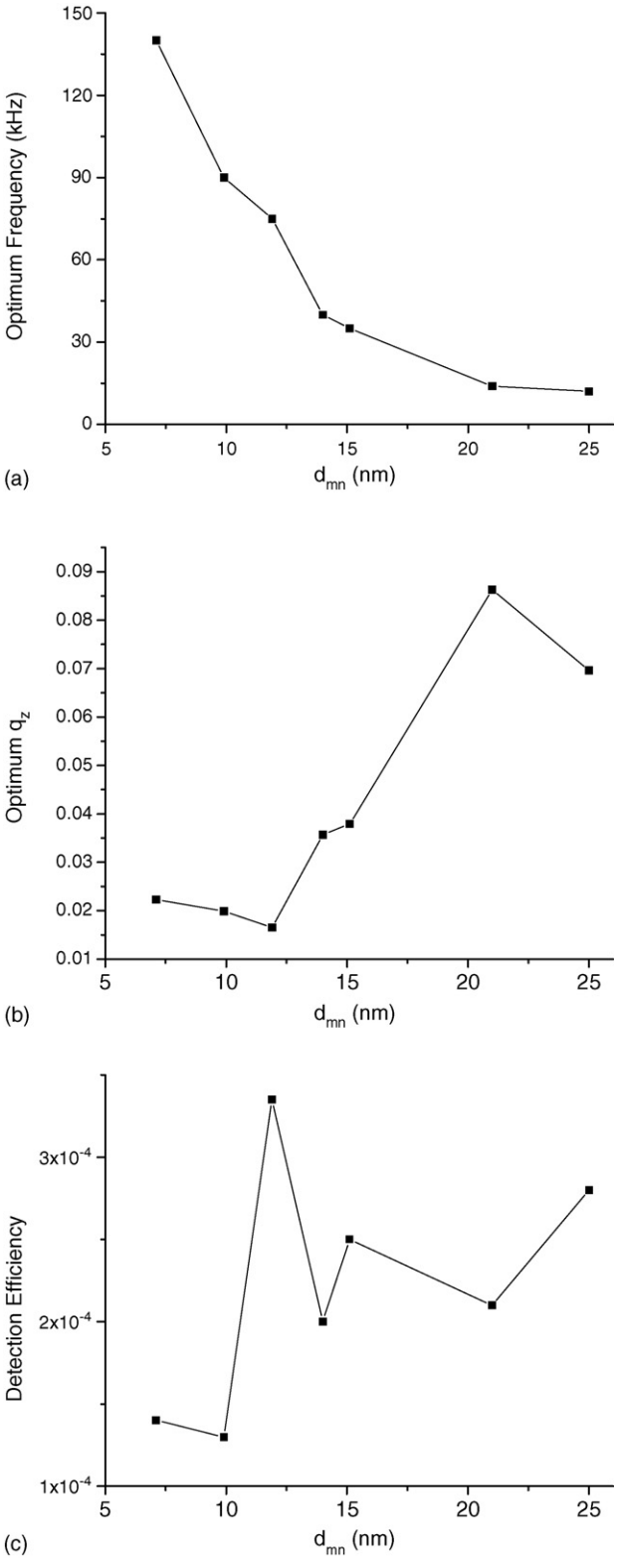

Fig. 3. (a) Optimum frequency (f_{opt}) for the ring electrode potential vs. mass normalized diameter (d_{mn}); (b) q_z for the optimum frequency vs. d_{mn}; (c) detection efficiency at the optimum frequency vs. d_{mn}.

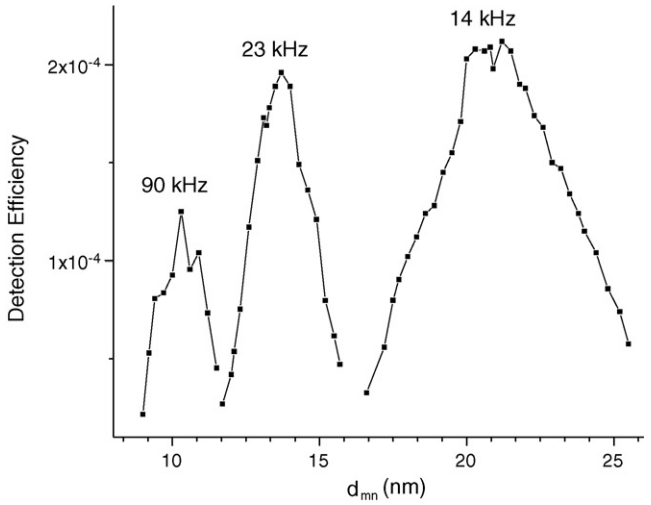

Fig. 4. Detection efficiency vs. normalized particle diameter (d_{mn}) for three different ring electrode frequencies. These plots correspond to geometric standard deviations of approximately 1.06 for 90 kHz, 1.09 for 23 kHz and 1.13 for 14 kHz.

ions, so it is possible for electron ionization of the background gas to occur without electron–ion recombination in the plasma. Indeed, we find that the background signal is larger when a particle is irradiated to produce a plasma than when no particle is in the laser beam path when the laser beam fires. This suggests that electrons from the plasma do play a role in ionization of background species.

With the digital ion trap, the ring electrode potential is fixed (+504 V) during the laser pulse and subsequent ion extraction from the trap. In contrast, the ring electrode potential in our previous work was sinusoidal and changed over this time period. As a result, the resolution and intensity of the time of flight spectrum with the sinusoidal potential is strongly dependent on the timing of the laser pulse during the sinusoidal cycle, and spectral calibration was sensitive to jitter or drift in this timing. The digital ion trap overcomes these problems since the ring electrode potential is fixed. Fig. 5a and b show the averaged mass spectra (average of 100 individual particle spectra) for d_{mn} ~9 nm (f = 100 kHz) sucrose particles. Fig. 5a was obtained with a reflector potential (L in Fig. 1) of +510 V, a value just above the acceleration potential. The acceleration potential is essentially given by the ring electrode potential (i.e., +504 V) since particles are irradiated in the center of the ion trap. In this spectrum, ions from the trapped particle(s) are C^{2+} (6 m/z), C^{3+} (4 m/z), C^{4+} (3 m/z), O^{2+} (8 m/z), O^{3+} (5.3 m/z), O^{4+} (4 m/z) and H^+ (1 m/z). Background ions include C^+ (12 m/z), CH^+ (13 m/z), H_2O^+ (18 m/z), N_2^+ (28 m/z), and Ar^+ (40 m/z) among others.

Changing the reflector potential L allows the kinetic energy distribution of the ions in Fig. 5a to be investigated. It is found that the energy distribution is much different for ions from the particle and background. Fig. 5b shows the mass spectrum of the same sucrose particles when the reflector potential (L) is decreased to +380 V. The background ions are completely eliminated and ions from the particle show only a slight decrease in intensity, suggesting that these ions have a substantial kinetic energy deficit. Both spectra in Fig. 5 were taken with the intermediate reflector potential (K in Fig. 1) of −230 V, which is the value for optimum ion focusing with L = +380 V. Therefore, the peak widths are much narrower in Fig. 5b than in Fig. 5a.

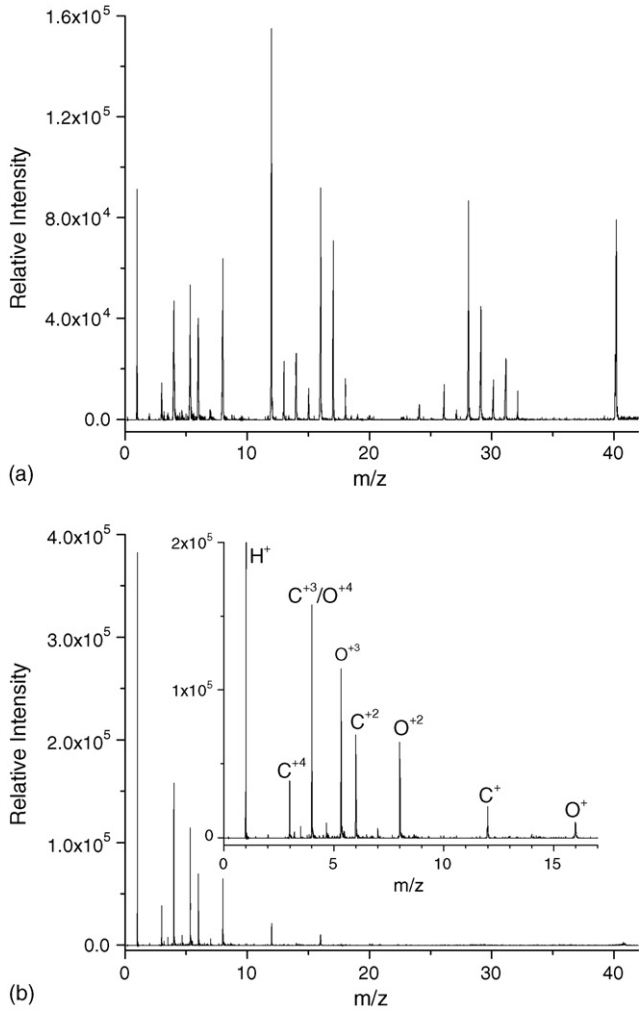

Fig. 5. (a) Averaged mass spectrum (100 individual particle spectra) of sucrose particles (d_{mn} = 9 nm; f = 100 kHz) taken with reflector potential L of +510 V; (b) averaged mass spectrum (100 individual particle spectra) of the same sucrose particles taken with a reflector potential L of +380 V. The inset of 'b' shows an expansion of the multiply charged ion region. The reflector potential K was −230 V for both spectra.

Fig. 6 summarizes the dependence of several particle and background ions on reflector potential. A kinetic energy deficit is observed for all ions, although the magnitude is greater for ions produced from the particle. The deficit is most readily explained by shielding of the ions from the electric field gradient by the laser induced plasma. Shielded ions that are initially traveling in the direction of the flight tube (i.e., in the direction of end cap G) receive less acceleration from the electric field and therefore acquire an energy deficit. Shielded ions that are initially traveling in the opposite direction (i.e., toward end cap E) would receive excess kinetic energy and are not detected with the range of reflector voltages used in this experiment. Shielded ions that are initially traveling toward the ring electrode receive no energy deficit or excess. Background ions exhibit a smaller energy deficit presumably because they are formed from lower

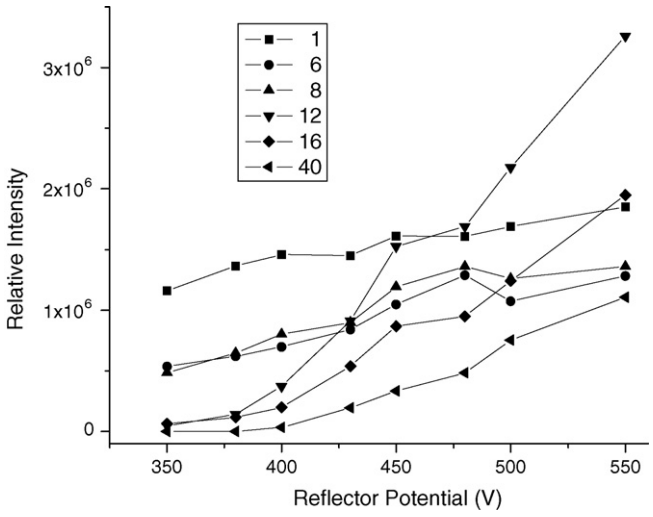

Fig. 6. Relative intensity (average of 100 individual particle spectra) vs. reflector potential L for several ions from the particle (8, 6 and 1 *m/z*) and background (40, 16 and 12 *m/z*). The particles are the same as in Fig. 4. The reflector potential K was −230 V for all experiments.

kinetic energy precursors and/or they are formed at a later time after the laser pulse when there is less opportunity for shielding from the acceleration potential.

While the ion dynamics in the laser induced plasma are complex and not all ions from the particle are necessarily detected, the elemental composition of the particle calculated from the mass spectrum is remarkably unaffected by the reflector potentials chosen. The procedure for determining the elemental composition was discussed in detail in our previous work [4]. Briefly, the carbon to oxygen mole ratio is determined by averaging the compositions determined from each charge state (+2 to +4) after deconvolution of the C^{3+} and O^{4+} contributions to the signal at 4 *m/z*. The measured carbon to oxygen mole ratios are independent of reflector potential across the range studied in Fig. 6. The measurements give an average of 1.1 ± 0.1, which matches the ratio expected from the molecular formula ($C_{12}H_{22}O_{11}$). As noted in our previous work, the carbon to hydrogen signal intensity ratio does not accurately reflect the mole ratio. For the reflector voltages in Fig. 6, the measured signal intensity ratio decreases from 0.74 at +350 V to 0.30 at +550 V.

The ability to determine the oxygen content of organic particles is further demonstrated in Table 2 where the expected and measured carbon to oxygen ratios for sucrose, polyethylene glycol (PEG) and polypropylene glycol (PPG) particles are tabulated for repetitive measurements using "standard" reflector potentials (K = −175 V and L = +510 V). The spectra of PEG and PPG are similar to those Fig. 5 except that the relative intensities of the carbon and oxygen ions are different. The measured mole ratios are consistently within +5% of the expected values.

Table 2
Measured and expected mole ratios for several particle compositions

Composition	Mole ratio	Measured	Expected
Sucrose	C:O	1.06 ± 0.03	1.09
Polyethylene glycol	C:O	1.93 ± 0.04	2.00[a]
Polypropylene glycol	C:O	2.60 ± 0.04	2.62[a]
Sodium chloride	Na:Cl	1.02 ± 0.07	1.00
Ammonium sulfate	(S + O):N	2.50 ± 0.09	2.50

Range of particle diameters (d_{mn}) is 10–25 nm.
[a] Expected mole ratios include contribution of end groups.

Fig. 7 shows the mass spectra of three inorganic particle compositions, sodium chloride, ammonium nitrate and copper(II)

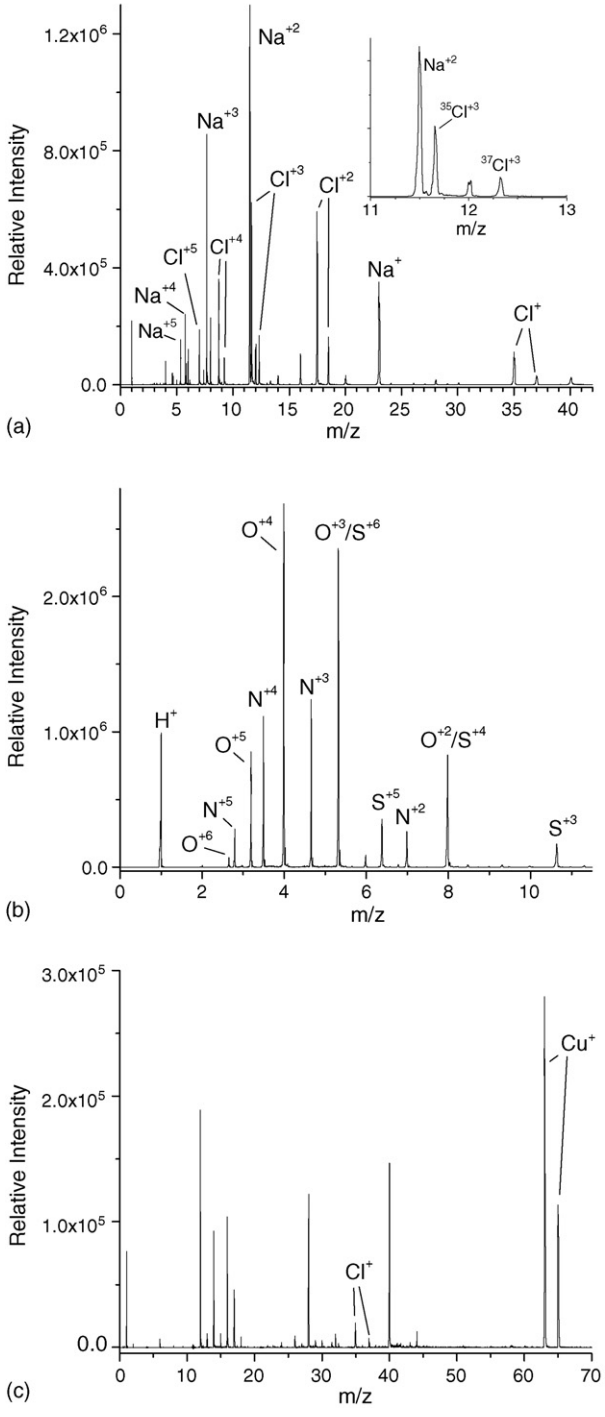

Fig. 7. Averaged mass spectra (100 individual particle spectra) of: (a) sodium chloride, d_{mn} = 16 nm (f = 25 kHz), (b) ammonium sulfate, d_{mn} = 20 nm (f = 15 kHz) and (c) copper(II) chloride, d_{mn} ~ 20 nm. The reflector potentials for each spectrum were K = −175 V and L = +510 V.

chloride. All three spectra were obtained with the "standard" reflector potentials. The mass spectra of sodium chloride and ammonium nitrate particles (Fig. 7a and b) are similar in character, showing atomic ions up to the +6 charge state. From the relative signal intensities of ions in the sodium chloride spectrum in Fig. 7a, the measured and expected ratios of Na:Cl agree within a few percent (Table 2). The resolving power, illustrated by the inset in Fig. 7a, is on the order of 320 at 11 *m/z*. The presence of a small amount of water and/or hydrocarbon impurity is indicated by multiply charged C and O ions as well as H^+. From the relative signal intensities of ions in the ammonium sulfate spectrum in Fig. 7b, the (S + O):N atomic ratio is readily determined and also agrees closely with the expected ratio (Table 2). As with sodium chloride, a small amount of hydrocarbon impurity is indicated by the presence of C^{2+}. The relative amounts of S and O are not deconvoluted in this work owing to signal overlap at 16, 8 and 5.3 *m/z*. The measured atomic ratios are independent of d_{mn} over the range studied, 10–25 nm. Note that the absolute signal intensities in Figs. 5a, 7a and 7b increase with increasing particle size.

Copper(II) chloride shows very different behavior from the other two salts. No multiply charged ions are observed in Fig. 7c—only Cu^+ and a small amount of Cl^+ are detected. The relative signal intensities do not match the expected ratio and the absolute signal intensity is much less than that of comparably sized sodium chloride or ammonium sulfate particles. This spectrum is characteristic of a conventional laser ablation experiment with a much lower laser fluence such that a laser induced plasma is not formed and cationic species are preferentially ionized. Evidently, plasma formation is quenched when this particle composition is irradiated. We have observed similar behavior for 60–100 nm diameter particles composed of iron and chromium salts. (Wang, Chen and Johnston, unpublished work.) It is possible that the high density of electronic states of transition metal atoms and/or the presence of water molecules in the particle dissipate the energy introduced by laser irradiation and prevent plasma formation.

The effective density of an aerosol can be determined if both d_m and d_{mn} are known (Eq. (1)). This determination is illustrated for sodium chloride particles that are size-selected with the SMPS. Sodium chloride particles with $d_m = 20$ nm are found to have $f_{opt} = 12$ kHz. Based on a polynomial fit of the data in Fig. 3a, this value of f_{opt} corresponds to $d_{mn} = 25$ nm. The density calculated from these values of d_m and d_{mn} is 2.0 g/cm^3 (bulk density of NaCl = 2.165 g/cm^3). While the measured and bulk values are close, additional experiments will be required to assess whether the small difference can be linked to a nonspherical particle shape of the sodium chloride aerosol or if it simply reflects of the accuracy/precision of the measurement.

4. Conclusion

The digital ion trap has several advantages for use with a time of flight mass analyzer to characterize nanoparticles. The amplitude and frequency of the ring potential are easily manipulated, extraction of atomic ions from the ion trap into the time of flight analyzer is easily optimized, and the reflector potential can be manipulated to remove background ions. The current setup permits efficient trapping and analysis of particles with mass normalized diameters between about 7 and 25 nm in diameter. Extending the trapping range to larger and smaller particles should be possible through manipulation of the bath gas conditions and potentials.

Acknowledgements

This research was supported by grants from the United States Environmental Protection Agency (R829622010) and National Science Foundation (CHE-0517972). Although the research described in this article was funded in part by the U.S.E.P.A., it has not been subjected to the Agency's required peer and policy review and therefore does not necessarily reflect the views of the Agency and no official endorsement should be inferred.

References

[1] P. Biswas, C.-Y. Wu, J. Air Waste Manage. Assoc. 55 (2005) 708.
[2] G. Oberdorster, E. Oberdorster, J. Oberdorster, Environ. Health Persp. 113 (2005) 823.
[3] M. Kulmala, H. Vehkamaki, T. Petaja, M. Dal Maso, A. Lauri, V.-M. Kerminen, W. Birmili, P.H. McMurry, J. Aerosol Sci. 35 (2004) 143.
[4] S. Wang, C.A. Zordan, M.V. Johnston, Anal. Chem. 78 (2006) 1750.
[5] J.A. Richards, R.M. Huey, J. Hiller, Int. J. Mass Spectrom. Ion Phys. 12 (1973) 317.
[6] L. Ding, M. Sudakov, S. Kumashiro, Int. J. Mass Spectrom. 221 (2002) 117.
[7] L. Ding, M. Sudakov, F.L. Brancia, R. Giles, S. Kumashiro, J. Mass Spectrom. 39 (2004) 471.
[8] L. Ding, S. Kumashiro, Rapid Commun. Mass Spectrom. 20 (2006) 3.
[9] X. Wang, A. Gidwani, S.L. Girshick, P.H. McMurry, Aerosol Sci. Technol. 39 (2005) 624.
[10] D.-R. Chen, D.Y.H. Pui, S.L. Kaufman, J. Aerosol Sci. 26 (1995) 963.
[11] S.L. Kaufman, J.W. Skogen, F.D. Dorman, F. Zarrin, K.C. Lewis, Anal. Chem. 68 (1895) 1996.
[12] S.T. Quarmby, R.A. Yost, Int. J. Mass Spectrom. 190/191 (1999) 81.
[13] W.D. Reents, Z. Ge, Aerosol Sci. Technol. 33 (2000) 122.
[14] W.D. Reents, M.J. Schabel, Anal. Chem. 73 (2001) 5403.
[15] R. Mahadevan, D. Lee, H. Sakurai, M.R. Zachariah, J. Phys. Chem. A (2002) 106.
[16] D. Lee, K. Park, M.R. Zachariah, Aerosol Sci. Technol. 39 (2005) 162.